RSC Advances

Dynamic Article Links ►

Cite this: DOI: 10.1039/c3ra46118a

www.rsc.org/xxxxxx

PAPER

A novel ionic liquid for Li ion batteries – uniting the advantages of guanidinium and piperidinium cations

Nicolas Bucher,[#, a, b] Steffen Hartung,[#, a, b] Denis Yu,[a, d]
Maria Arkhipova,[#, e] Philipp Kratzer,[e] Gerhard Maas,[e] Madhavi Srinivasan,[a, c] Harry E. Hoster *[, a, b, d]

Received (in XXX, XXX) Xth XXXXXXXXX 20XX, Accepted Xth XXXXXXXXX 20XX
DOI: 10.1039/c3ra46118a

We report on the synthesis and the properties of *N*,*N*,*N*’,*N*’-tetramethyl-*N*”,*N*”-pentamethyleneguanidinium bis(trifluoromethylsulfonyl) imide (PipGuan-TFSI). The cation of this novel ionic liquid combines guanidinium and piperidinium structural elements. We tested it for its viscosity, (Li-)ion conductivity, and also for its thermal and electrochemical stability. Furthermore, a 0.5 M solution of lithium TFSI in PipGuan-TFSI was tested as an electrolyte for Li-ion batteries. These experiments included cycles of Li deposition/dissolution on stainless steel and (de-) intercalation into/from $LiFePO_4$ electrodes. The tests involving $LiFePO_4$ cathodes were performed at various C-rates and temperatures for a better quantitative comparison to other electrolyte systems. We discuss in how far PipGuan-TFSI successfully combines the advantages of guanidinium and piperidinium ionic liquids for battery electrolyte applications.

Introduction

Ionic liquids (ILs) are salts with a melting point below 100 °C. Room temperature ionic liquids, which is a subgroup defined by a melting point below room temperature, have attracted great interest in recent years as tunable “designer solvents”. ILs are electrochemically and thermally stable, have a negligible volatility, and thus a low flammability.[1,2] Those properties make them suitable not only for (sustainable) chemical synthesis[3] or carbon capture[4,5] but also for energy storage applications[6] such as super capacitors, batteries, fuel cells and solar cells.[2,7–12] The gain in safety due to the low volatility of ILs comes with a higher viscosity and concomitantly lower ion conductivity[13] as compared to traditional, molecular solvents. Furthermore, any IL to be used in electrochemical energy storage devices must exhibit a suitable stability window. Both the ion conductivity and the potential window are tackled by the design of new ionic liquids.[14–16]

IL based electrolytes in Li ion batteries (LIBs) are usually ternary mixtures containing Li^+ ions and the anions and cations of the respective IL. The Li salt and the IL thus share the same anion. Therefore, the IL cation becomes the subject of target oriented optimization. Common basic structures are pyridinium,[17] imidazolium,[18–21] ammonium,[20–23] sulfonium, pyrrolidinium,[20,21,24–26] guanidinium,[27–33]or piperidinium.[19–21,34,35] The infinite number of possible structural variations in combination with the substantial synthesis efforts calls for a systematic strategy. Parallel to computational studies that are on the way in many research groups,[14–16] there is an obvious demand for systematic synthesis variations in combination with a set of electrochemical benchmark tests. For substances whose properties are already close to the desired optimum, variations can be incremental, e.g., modifying moieties of existing cation structures. For substances with more room for improvement, however, more substantial yet still systematic variations may speed up the progress – in analogy to Nature’s principles of genetic crossing that was successfully transferred to the field of multi-parameter optimization problems.

In this paper, we will demonstrate how the advantages of two different structural elements can be combined towards a new cation with better key properties than the parent structures. The two original structural elements are guanidinium and piperidinium. Guanidinium cations can be modified at six different sides and the resulting ILs have low viscosities. Main drawback of guanidinium cations, however, is their lack of electrochemical stability at the negative potential limit.[23,27,29,30] Piperidinium based ILs, on the other hand, were reported to have electrochemical windows exceeding 5 V and high cathodic stability versus lithium metal. Moreover, piperidinium ILs have a high thermal stability, which is crucial with regard to safety.[34,36] In the first part of this paper we will describe the synthesis of a new cation in which one side arm of a guanidinium cation was substituted with a piperidinium ring (PipGuan, see Fig. 1). Being initially synthesised as PipGuan chloride, an anion exchange towards PipGuan bis(trifluoromethylsulfonyl)imide (TFSI) yields a new IL, PipGuan-TFSI.

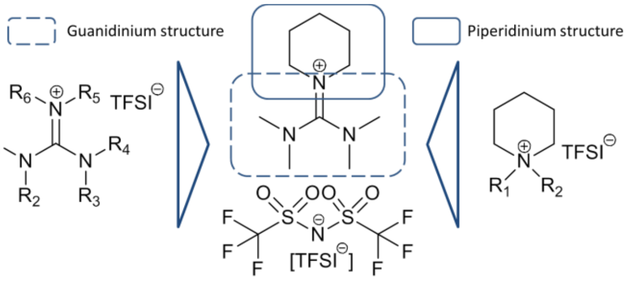

Fig. 1 *N,N,N′,N′*-Tetramethyl-*N″,N″*-pentamethyleneguanidinium bis(trifluoromethylsulfonyl)imide (PipGuan-TFSI).

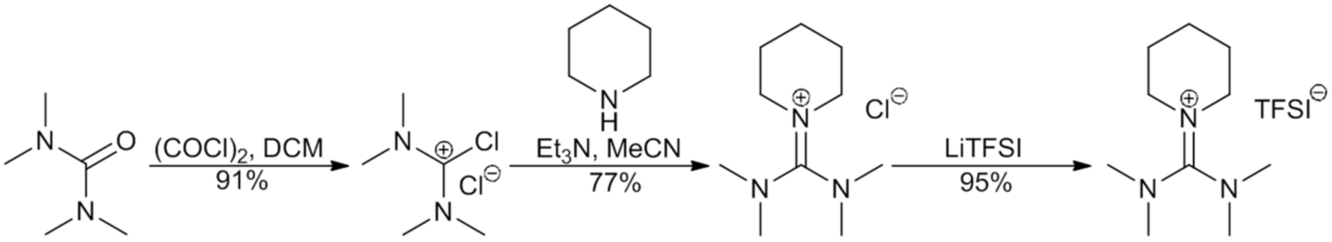

Fig. 2 Synthesis route to PipGuan-TFSI

We will then elucidate the physical and electrochemical properties of this IL. Those characterisations include Nuclear Magnetic Resonance (NMR) and Infrared (IR) spectrometry, Thermogravimetric analysis supported by mass spectroscopy (TGA-MS), Differential Scanning Calorimetry (DSC), and viscosity and conductivity measurements. The electrochemical properties were tested by cyclic voltammetry (CV) and Electrochemical Impedance Spectroscopy (EIS). Finally, we tested a solution of LiTFSI in PipGuan-TFSI as an electrolyte for a $LiFePO_4$ battery half-cell and compared the results at two different temperatures to the behaviour of the same cell using a commercial electrolyte. We will discuss in which respect the properties of the new cation structure reflect a compromise between the two parent structures and where the product of the crossing is superior to either of them.

Materials and Methods

Synthesis

The novel guanidinium-based ionic liquid *N,N,N',N'*-tetramethyl-*N",N"*-pentamethyleneguanidinium bis(trifluoromethylsulfonyl) imide was synthesised from tetramethylurea by partially modifying reported procedures (Fig. 2).[28,31] Rigorously dried organic solvents were used. All amines were dried with KOH pellets and stored under an argon atmosphere. ^{1}H NMR spectra were referenced to the residual proton signal of the solvent [$\delta(CDCl_3) = 7.26$ ppm]. ^{13}C spectra were referenced to the solvent signal [$\delta(CDCl_3) = 77.00$ ppm], and ^{19}F spectra to external C_6F_6 [$\delta(C_6F_6) = -162.9$ ppm].

As a first step, *N,N,N',N'*-tetramethylchloroformamidinium chloride was obtained by a dropwise addition of tetramethylurea (20 mL, 167 mmol) to freshly distilled oxalyl chloride (15.7 mL, 183 mmol) dissolved in 20 mL of dry dichloromethane at room temperature. The solution was stirred overnight and the solvent was removed under vacuum. The remaining precipitate was washed several times with dry diethyl ether until the washing ether was colourless. The solid *N,N,N',N'*-tetramethylchloroformamidinium chloride was dried for three hours at 20 ^{o}C/0.05 mbar to yield 27.09 g (95%) as a white moisture sensitive powder.

N,N,N',N'-Tetramethyl-*N",N"*-pentamethyleneguanidinium chloride was prepared by dropwise addition of a solution of piperidine (2.5 mL, 25 mmol) and triethylamine (3.5 mL, 25 mmol) in 20 mL of dry diethyl ether to a solution of *N,N,N',N'*-tetramethylchloroformamidinium chloride (4.3 g, 25 mmol) in 40 mL of dry acetonitrile at 0 °C. The mixture was stirred overnight at room temperature. The precipitated triethylammonium chloride was filtered off, and the solvents were distilled on the rotary evaporator. A 0.1 M NaOH solution was added to the residual oil, until the pH was slightly alkaline. To remove the coloured impurities, the aqueous solution was washed several times with diethyl ether. Volatile components were distilled on the rotary evaporator (40 °C/70 mbar) and the solid residue was subsequently dried at 50 °C/0.05 mbar. Afterwards, it was dissolved in dry acetonitrile/diethyl ether (2 : 1 *v*/*v*, 10 mL) and the solid was filtered off. The organic solvents were removed and the product was dried for 8 h at 80 °C/0.05 mbar. Crystallisation from ethyl acetate / dimethyl formamide (2 : 1) gave 4.2 g of *N,N,N',N'*-tetramethyl-*N",N"*-pentamethyleneguanidinium chloride (77% yield) as a white hygroscopic powder.

N,N,N',N'-Tetramethyl-*N",N"*-pentamethyleneguanidinium bis(trifluoromethylsulfonyl)imide (PipGuan-TFSI) was synthesised by anion exchange. Lithium bis(trifluoromethylsulfonyl)-imide (2.9 g, 10 mmol) and *N,N,N',N'*-tetramethyl-*N",N"*-pentamethyleneguanidinium chloride (2.2 g, 10 mmol) were dissolved in 30 and 10 mL, respectively, of deionised water. The solutions were combined resulting in two phases. After stirring the mixture at 70 °C for 30 min, it was cooled to room temperature, and dichloromethane (30 mL) was added. The organic phase was separated and washed with several portions of deionised water until chloride could not be detected any more in the rinsing water using $AgNO_3$. The organic phase was dried with Na_2SO_4, stirred over charcoal for 15 min, and filtered. The solvent was removed on a rotary evaporator, and the product was dried for 8 h at 120 °C/0.05 mbar. *N,N,N',N'*-Tetramethyl-*N",N"*-pentamethyleneguanidinium bis(trifluoromethylsulfonyl)-imide was obtained as a slightly yellowish oil (4.4 g, 95% yield).

Physical and Electrochemical Characterisation

NMR spectra were recorded on a Bruker DRX 400 spectrometer (^{1}H: 400.13 MHz; ^{13}C: 100.61 MHz; ^{19}F: 376.46 MHz). IR spectra were recorded with a Bruker Vector 22 FTIR spectrometer. Thermal stability was determined by TGA (Mettler Toledo STARe TGA/DSC1; Mettler-Toledo TGA/SDTA 851 for *N,N,N',N'*-tetramethyl-*N",N"*-pentamethyleneguanidinium chloride), the decomposition point was defined as $T_{\text{dec}} \hat{=}$ temperature of highest decomposition gradient at a heating rate of 5 K min^{-1}. The decomposition products were detected by mass spectrometry (Pfeiffer Vacuum Thermostar GSD320). Differential scanning calorimetry was performed with a Perkin Elmer DSC 7 instrument. Microanalyses were obtained with an Elementar vario MICRO cube instrument. Lithium bis(trifluoromethylsulfonyl)imide for synthesis was received from Acros Organics or IoLiTec GmbH with a purity of 99 %. Viscosity was measured using a Rheometer (Anton Paar GmbH, Rheometer

MCR 501), conductivity was measured using a conductivity meter (Eutech Instruments, CyberScan 600 Series). The electrochemical window was measured by linear sweep voltammetry (scan rate: 10 mV s^{-1}) in two different cells: (i) a two-electrode 2016 coin cell with stainless steel as the working electrode and lithium as the counter and reference electrode and (ii) a three-electrode beaker cell with glassy carbon as the working, Ag|AgNO$_3$ as the reference, and platinum as the counter electrode. For the reference electrode, a Ag wire was immersed in a solution of 0.01 M AgNO$_3$ in acetonitrile, with 0.1 M N(octyl)$_4$BF$_4$ as conducting salt. A junction with the compartment containing the IL was realized with a vycor glass frit. For both set-ups, the electrochemical windows were calculated for the cut-off current densities 0.1 mA cm^{-2} and 0.5 mA cm^{-2}. EIS was performed in a symmetric lithium coin cell set-up (Li|Electrolyte|Li). Plating/stripping experiments were conducted using a 2016 coin cell set-up with lithium metal and stainless steel electrodes. For both measurements, a Biologic VMP3 potentiostat was used. Battery tests were performed with an electrolyte consisting of the synthesised PipGuan-TFSI and 0.5 M lithium bis(trifluormethylsulfonyl)imide (LiTFSI, SOLVAY, 99.99%). Note that the maximum concentration attainable at 300 K was 0.8 M. Commercial lithium iron phosphate (LFP, ENAX) was used as cathode material. The composite cathodes were prepared by mixing LFP, acetylene black (Alfa Aesar, > 99%), and polyvinylidene fluoride (PVdF, Arkema, Kynar HSV 900) binder in the weight ratio of 80:10:10, with *N*-methyl-2-pyrrolidone (NMP, Sigma Aldrich, ≥ 99%), to form a slurry. The well-mixed, homogenous mixture was coated on an Al foil using a doctor blade, and dried at 80 °C in air to remove the solvent. Circular pieces with 16 mm diameter were punched out of the coated Al foil and roll-pressed between twin rollers to improve adherence of the coating to the Al foil. After drying the electrodes for 4 h under vacuum at 110 °C, the electrodes were assembled in a half-cell configuration in 2016 coin cells, using 16 mm circular lithium metal pieces as the anode, separated by a glass fibre separator (Whatman) swollen with the aforementioned electrolyte. Charge/discharge experiments were carried out with an Arbin battery tester. All measurements were performed with the purified and dry ionic liquid. Magnetic resonance techniques (1H-NMR, 13C-NMR, 19F-NMR), infrared spectroscopy, mass spectroscopy, Karl-Fischer analysis and elemental analysis did not indicate the presence of any impurities other than small traces of water (according to Karl-Fischer: < 50 ppm).

Results and Discussion

Analytical Data

***N,N,N’,N’*- Tetramethylchloroformamidinium chloride:**
^{1}H NMR (CDCl$_3$): δ = 3.55 (s, 12 H, NC*H*$_3$) ppm.

***N,N,N’,N’*-Tetramethyl-*N”,N”*-pentamethyleneguanidinium chloride**

Melting point = 158–159 °C, T_{dec} = 330 °C, ^{1}H NMR (CDCl$_3$): δ = 1.25–1.50 (m, 6 H, CH$_2$(C*H*$_2$)$_3$CH$_2$, pip), 2.77 (s, 12 H, NC*H*$_3$), 2.97–3.13 (m, 4 H, NC*H*$_2$, pip) ppm. ^{13}C NMR (CDCl$_3$): δ = 22.6 (N(CH$_2$)$_2$*C*H$_2$, pip), 24.5 (NCH$_2$*C*H$_2$CH$_2$, pip), 40.05 und 40.09 (N*C*H$_3$), 49.3 (N*C*H$_2$CH$_2$CH$_2$, pip), 161.9 (*C*N$_3$) ppm. IR (ATR): ν = 2930 (m), 2856 (m), 1564 (s), 1435 (m), 1407 (s), 1277 (m), 1253 (m) cm^{-1}. MS (CI): *m*/*z* = 184 (100%, [cation]$^+$). Anal. calcd. for $C_{10}H_{22}ClN_3$*0.75H$_2$O: C 51.49, H 10.15, N 18.01; found: C 51.48, H 10.27, N 17.94.

***N,N,N’,N’*-Tetramethyl-*N”,N”*-pentamethyleneguanidinium bis(trifluoromethylsulfonyl)imide (PipGuan-TFSI)**

Melting point = 3 °C, T_{dec} = 463 °C, ^{1}H NMR (CDCl$_3$): δ = 1.65-1.80 (m, 6 H, CH$_2$(C*H*$_2$)$_3$CH$_2$, pip), 2.98 and 2.99 (2 s, 6 H each, NC*H*$_3$), 3.20–3.35 (m, 4 H, NC*H*$_2$, pip) ppm. ^{13}C NMR (CDCl$_3$): δ = 23.4 (N(CH$_2$)$_2$*C*H$_2$, pip), 25.1 (NCH$_2$*C*H$_2$CH$_2$, pip), 40.32 und 40.35 (N*C*H$_3$), 49.9 (N*C*H$_2$CH$_2$CH$_2$, pip), 162.8 (*C*N$_3$) ppm. ^{19}F NMR (CDCl$_3$): δ = -75.3 ppm. IR (NaCl): ν = 2951 (m), 2864 (m), 1569 (s), 1411 (m), 1347 (s), 1330 (s), 1176 (s), 1134 (s), 1053 (s) cm^{-1}. MS (CI): *m*/*z* = 184 (100%, [cation]$^+$). Anal calcd. for $C_{12}H_{22}F_6N_4O_4S_2$ (464.44): C 31.03, H 4.77, N 12.06; found: C 31.03, H 4.68, N 12.25.

Thermal properties of PipGuan-TFSI

DSC revealed a melting point is 3 °C as measured by DSC. It is lower than the one of *N,N*-diethyl-*N',N',N'',N''*-tetramethyl - or *N,N,N',N'*-tetramethyl *N*”,*N*”-dipropylguanidinium-TFSI (9.9 and 12.9 °C, respectively) but slightly higher than the one of *N,N,N',N'*-tetramethyl-*N*”-ethyl-*N*”-propylguanidinium-TFSI (-1.6 °C).[29,30] In general, the melting point of ionic liquids increases for more symmetrical cations, because symmetry facilitates a closer packing of the ions. Leaving the methyl groups at *N* and *N’* constant, the melting point tends to decrease with increasing chain length of the alkyl chain at *N”*, up to a critical molar mass.[30] Considering that the piperidinium contains five carbon atoms, the relative position of the melting point of PipGuan-TFSI is within the expected range.

TGA showed that PipGuan-TFSI is stable up to 415 °C (5% of mass loss). The temperature of highest decomposition gradient is at 463 °C. The mass spectra of the decomposition products were analysed at the onset, in the middle, and at the end of the decomposition (Fig. 3). In the beginning, the fragments seem to indicate the decomposition mainly of the cation (Fig. 3a), whereas at the end, the fragments are predominantly decomposition products of the anion (Fig. 3b). In the middle of decomposition, fragments from both cation and anion are present (Fig. 3c). Thus, it can be assumed that the cation is the limiting ion for thermal stability. Comparing this data with other ILs, PipGuan-TFSI is thermally more stable than other guanidinium ILs, but less stable than piperidinium based ILs.[30,34]

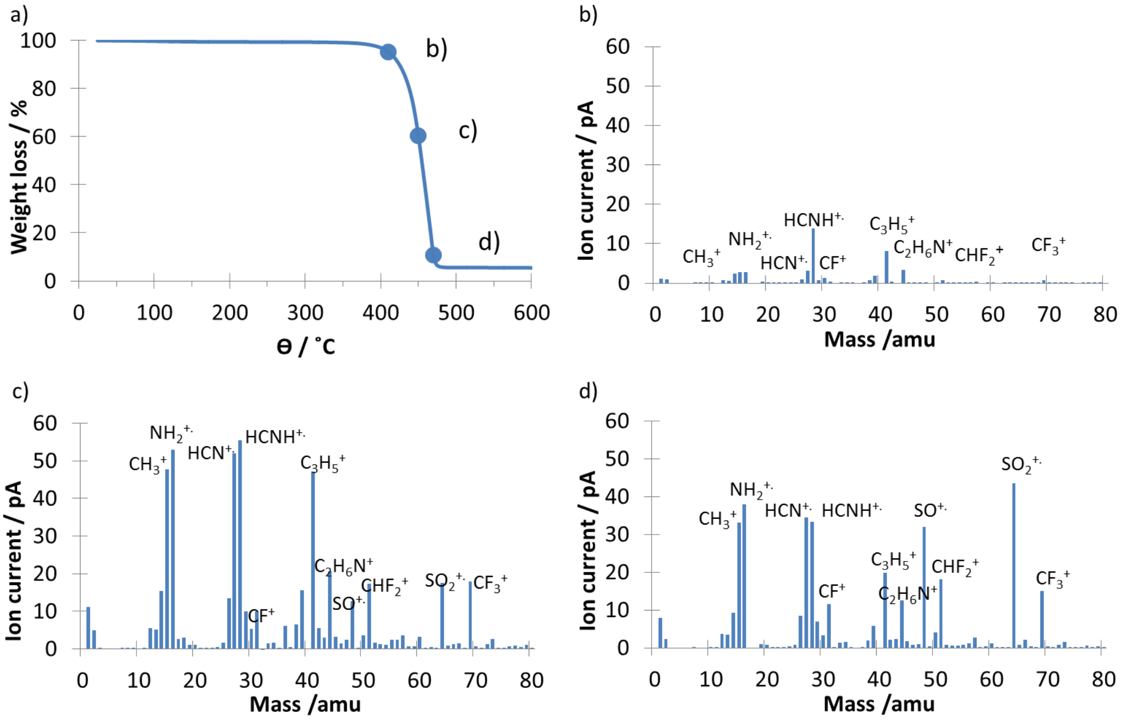

Fig. 3 a) TGA of PipGuan-TFSI (5 K min^{-1}), b) MS of PipGuan-TFSI at 410 °C, c) MS of PipGuan-TFSI at 450 °C, d) MS of PipGuan-TFSI at 470 °C

Viscosity and Conductivity

Viscosities and conductivities were measured for pure PipGuan-TFSI and for a solution of 0.5 M LiTFSI, a potential LIB electrolyte. As found in similar systems,[9,27] the viscosity of the Li$^+$ containing solution is higher than that of the pure IL for all temperatures. For both samples, the viscosity decreases with increasing temperature (Fig. 4) according to a Vogel-Tammann-Fulcher relationship (Eq. 1);[37,38] for the fitted parameters see Table 1.

$$\eta = \eta_0 \; exp\left(\frac{B}{T-T_0}\right) \qquad (Eq. 1)$$

The values are comparable to those reported for hexaalkyl guanidinium-based ionic liquids with TFSI as the anion.[30]

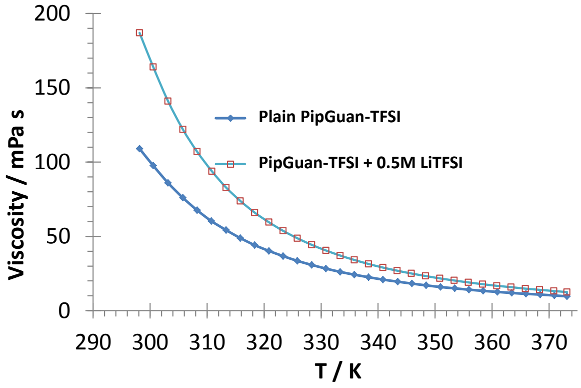

Fig. 4 Temperature dependence of viscosity for PipGuan-TFSI and 0.5 M solution of LiTFSI in PipGuan-TFSI

Room temperature viscosities of previously reported hexaalkyl guanidinium[30] and piperidinium[34] based ILs are in the range of 58–113 mPa·s and 190–370 mPa·s, respectively. For PipGuan-TFSI, our measurements reveal 108 mPa s at 25 °C. As expected, this value lies between those for guanidinium and piperidinium. The viscosity of the 0.5 M LiTFSI electrolyte was found to be 164 mPa·s at room temperature.

Conductivities were measured in an Ar filled glovebox at 28 °C. The measurements revealed 1.46 mS cm^{-1} and 0.74 mS cm^{-1} for pure PipGuan TFSI and the 0.5 M LiTFSI electrolyte, respectively. Again, the conductivity of the pure IL lies between the value ranges reported for *N*,*N*,*N'*,*N'*-tetramethyl-*N''*-alkyl^1-*N''*-alkyl^{2}guanidinium-TFSI (alkyl$^{1/2}$ = methyl, ethyl, propyl and butyl), which are 1.02–2.86 mS cm^{-1} (at 25 °C),[30] and for *N*-alkyl^1-*N*-alkyl^{2}piperidinium-TFSI (alkyl$^{1/2}$ = methyl, ethyl, propyl, butyl, pentyl, hexyl, or heptyl), which are 2.1·10^{-5}–0.92 mS cm^{-1} (at 20 °C)[34], respectively.

Table 1 Parameters for the Vogel-Taman-Fulcher equation for PipGuan-TFSI and the electrolyte (0.5 M solution of LiTFSI in PipGuan-TFSI)

	η_0 / mPa s	B / K	T_0 / K	R^2
PipGuan-TFSI	0.26 ± 7%	705 ± 2%	190 ± 1%	>0.9999
Electrolyte	0.17 ± 9%	797 ± 3%	174 ± 1%	>0.9999

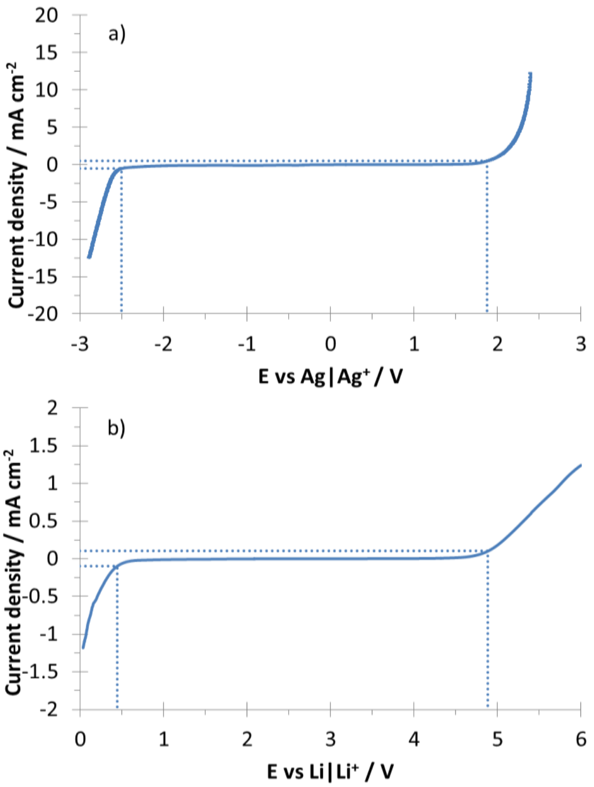

Fig. 5 a) Electrochemical window of PipGuan-TFSI using a 3-electrode set-up with Ag|AgNO$_3$ as reference, glassy carbon as working and Pt as counter electrode, b) Electrochemical window of PipGuan-TFSI using a coin cell set-up with Li as combined counter&reference and stainless steel as a working electrode; the dotted lines represent a cut-off current density of 0.5 mA cm^{-2} for a), and 0.1 mA cm^{-2} for b).

Electrochemical measurements

Figs. 5a and 5b show the electrochemical window of PipGuan-TFSI measured in two different ways. Fig. 5a was measured with a three-electrode set-up, with glassy-carbon as the working, Ag|AgNO$_3$ as the reference, and platinum as the counter electrode. The three-electrode set-up shows an electrochemical window of 4.40 V between -2.55 V and 1.85 V vs. Ag|Ag$^+$, all for a cut-off current density of 0.5 mA cm^{-2}. For a cut-off at 0.1 mA cm^{-2}, the window narrows to 4.16 V with -2.50 V and 1.66 V vs. Ag|Ag$^+$ as cathodic and anodic limits, respectively (see Table 2). Fig. 5b was measured in a coin cell to simulate working conditions in a LIB. The two-electrode set-up with stainless steel as a working and Li metal as a counter electrode showed an electrochemical window of 5.11 V (0.2 V … 5.31 V) for a cut-off current density of 0.5 mA cm^{-2}, and of 4.44 V (0.44 V… 4.88 V) for a cut-off at 0.1 mA cm^{-2}.

Table 2 Electrochemical stability limits and electrochemical window for PipGuan-TFSI

	2 Electrodes, vs. Li|Li$^+$		3 Electrodes, vs. Ag|Ag$^+$	
Cut-off current density / mA cm $^{-2}$	0.1	0.5	0.1	0.5
Anodic limit / V	4.88	5.31	1.66	1.85
Cathodic limit / V	0.44	0.20	-2.50	- 2.55
Electrochem. window / V	4.44	5.11	4.16	4.4

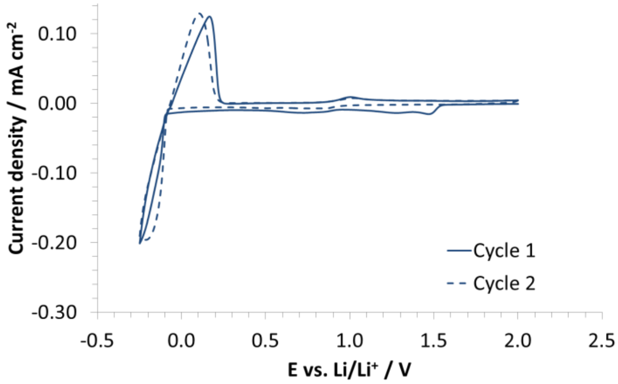

Fig. 6 Cyclic voltammogram for 0.5 M LiTFSI in PipGuan-TFSI in coin cell set-up with stainless steel as a working and Li as a combined counter&reference electrode, respectively. Scan rate 0.3 mV s^{-1}.

It should be pointed out that the Li reference potential obtained in these cells is not well-defined because there is no controlled Li$^+$ content in the Li-TFSI solution as required for a true Li/Li$^+$ system.[39] Nevertheless, the upper potential limit indicates that PipGuan-TFSI could be suitable for high-voltage battery cells.

For an application of PipGuan-TFSI in Li-ion batteries the electrochemical properties of the Li$^+$ containing electrolyte (PipGuan-TFSI + 0.5 M LiTFSI) are more important than those of the plain IL. Fig. 6 shows the first and second cycle of a freshly mounted coin cell with stainless steel and lithium as working and combined counter&reference electrode, respectively. Starting at 2 V, the first CV cycle shows broad cathodic features starting at 1.5 V in the negative going scan. Those presumably reflect electrolyte decomposition, in analogy to previous observations for other ILs.[27,24,40,41]

The fact that these features are only observed in the first negative going scan indicates that the product is a passivating layer (sometimes referred to as solid electrolyte interphase, SEI). In following cycles, no major features are visible until -0.08 V. Integration of oxidation and reduction charges shows that for the scan from -0.08 V to -0.25 V and back, the total cathodic charge adds up to about twice the total anodic charge that is re-gained above -0.08 V. The anodic charge is assigned to the stripping of Li layers that were plated onto the stainless steel electrode at $E <$ -0.08 V. The cathodic charge thus splits into contributions from Li plating and electrolyte decomposition in coarsely equal shares. Scans to lower E revealed a more pronounced increase of the negative as compared to the positive charge in the anodic counter-peak, indicating that electrolyte decomposition becomes dominating at more negative potentials. Comparing the CV in Fig. 6 with the linear sweep scan of the plain IL in Fig. 5b, the onset of electrolyte decomposition seems to be shifted to more negative potentials in the presence of Li$^+$ ions in the solution.

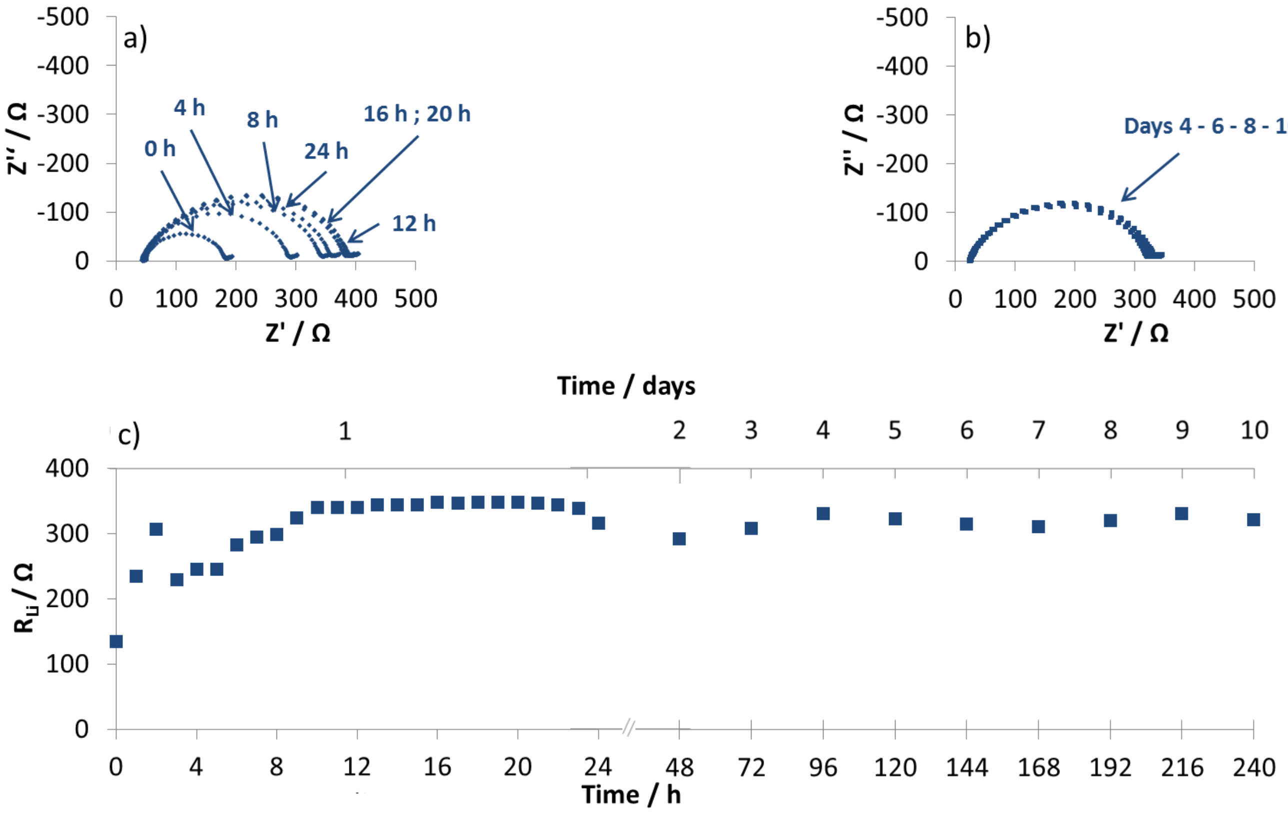

Fig. 7 Impedance response of a symmetrical Li|0.5 M LiTFSI in PipGuan-TFSI|Li cell stored at room temperature during the first a) 12 hours, b) 10 days, c) time evolution of R_{Li}

It was speculated previously that the addition of LiTFSI enables the formation of a passivating layer that widens the potential window.[40,41] In-depth studies on the composition of this layer have been conducted earlier by other groups.[42–44]

As highlighted above, however, the Li based reference potentials in the plain and in the LiTFSI containing IL should not be directly compared: if the potential determining equilibrium reaction is $Li_{solid} \leftrightarrow Li^+ + e^-$, the Li^+ concentration in the neat IL is undefined and can easily be several orders of magnitude below the one in the electrolyte with 0.5 M LiTFSI.[39] According to the Nernst equation the pseudo-reference potential in the neat IL can thus be several multiples of 60 mV more negative than the Li/Li$^+$ potential in the electrolyte. Such a shift could be the main reason for the different onset potentials for cathodic IL decomposition without (Fig. 5b) and with (Fig. 6) LiTFSI in the solution. IUPAC recommends the utilization of dissolved redox couples (e.g., ferrocene/ferrocenium) as internal references in such systems.[39,45–47] Using this method, we seek to clarify the actual effect of LiTFSI on the width and potential stability window in upcoming experiments. As to the potential scale in Fig. 6, one should also emphasise that Li deposition and dissolution is setting in at -0.08 V in the negative and positive going scan, respectively, and not at 0 V as one should expect. This means that the Li/Li$^+$ potential is more negative for the freshly deposited Li film than for the Li foil used as combined counter&reference electrode. We tentatively assign this potential difference to a chemical modification of the surface of the Li foil due to (electro-)chemical side reactions as they will be discussed in more detail below. Apart from the open questions related to the electrochemical equilibrium potentials, however, the Li plating/stripping behaviour in Fig. 6 confirms transport of Li$^+$ between the two electrodes and thus the suitability of PipGuan-TFSI as electrolyte solvent for Li-ion batteries.

Apart from the Li$^+$ transport properties and the potential dependent electrochemical stability of PipGuan-TFSI we also studied its interaction with metallic Li. Specifically, we used EIS to analyse the charge transfer properties of the interface between metallic Li and PipGuan-TFSI + 0.5 M LiTFSI. Fig. 7 shows the evolution of the impedance response of a cell that was stored at room temperature under open circuit conditions, just interrupted by the EIS measurements. The intercept of the semicircles at high frequencies (left side) was associated with the bulk resistance. The difference between the two intercepts with the real axis was interpreted as the electrode-electrolyte resistance (R_{Li}), combining both the charge transfer and the passivating layer resistance. Of these two components, R_{Li} is probably dominated by the resistance of the passivating layer.[17,48,49]As can be seen from Fig. 7a, resistance stabilised after 12 hours. Fig. 7b shows the long-term impedance test over 10 days, which shows only little change in the R_{Li} resistance. This indicates that a passivating layer is forming at the lithium electrode during the first 12 hours, and that it stays stable afterwards. Due to the open circuit conditions, this formation must be a chemical or a corrosion type of reaction.

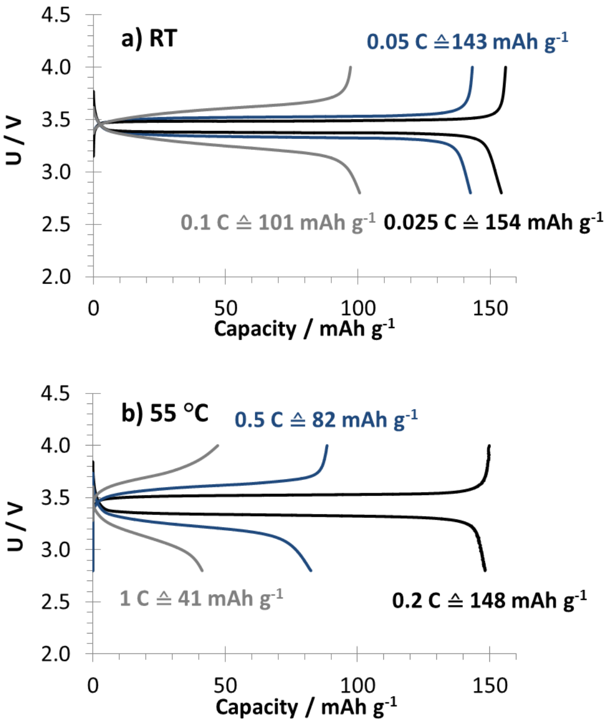

Fig. 8 Charge/discharge behaviour of 0.5 M LiTFSI in PipGuan-TFSI in a coin cell with lithium iron phosphate and lithium electrodes; a) 24 °C, b) 55 °C.

To complete the picture of PipGuan-TFSI as a suitable electrolyte solvent for Li-ion batteries we examined the charge/discharge behaviour of $LiFePO_4$ half cells at different C-rates and two different temperatures (24 and 55 °C). Fig. 8a shows a discharge capacity of 154 mAh g^{-1} for charge/discharge at 0.025 C. The same capacity was found in a test experiment with the same electrodes and commercial electrolyte (EC:DMC, 1 M $LiPF_6$) at 0.2 C. For 0.05 C and 0.1 C, the discharge capacities attained with the PipGuan-TFSI based electrolyte reduce to 143 mAh g^{-1} and 101 mAh g^{-1}, respectively. Such a negative correlation of C-rate and capacity is commonly observed and attributed to the high viscosity of ionic liquids.[9,19,50] This assignment fits to the observed charge/discharge behaviour at 55 °C (Fig. 8b), where a capacity of 148 mAh g^{-1} is reached at 0.2 C. This capacity is almost 150 % of the value obtained at 0.1 C and 24 °C. Furthermore, it is about the same capacity as we could reach for an identical half cell with standard electrolyte (1 M $LiPF_6$ in EC/DMC) at the same C-rate and at 24 °C (curve not shown here). In summary, the data in Fig. 8 indicate that the main disadvantage of PipGuan-TFSI as an electrolyte solvent for Li-ion batteries is a poor Li^+ conductivity due to a high viscosity. Increasing the temperature to 55 °C lowers the viscosity by about a factor of four, which must be the reason for the improved half-cell performance at that temperature.[29] Furthermore, the achieved discharge capacities for PipGuan-TFSI based electrolyte (143 mAh g^{-1} at 0.05 C, 101 mAh g^{-1} at 0.1 C at 24 °C) lay above the values of 93 mAh g^{-1} (0.05 C) and and 80 mAh g^{-1} (0.1 C) that were reported for *N*-methyl-*N*-butylpiperidinium-TFSI[19] and *N*,*N*,*N*',*N*'-tetramethyl-*N*”-butyl-*N*”-methylguanidinium-TFSI,[32] respectively. In this respect, the performance of the PipGuan-TFSI based electrolyte does not lie between the two classes of material but is better than the respective individual performances.

Conclusions

A new ionic liquid that combines the structures of piperidinium and guanidinium based ionic liquids, PipGuan-TFSI, has been synthesised. The physical properties, i.e., thermal stability, viscosity and conductivity of this new material lie between these two different classes of ionic liquids. PipGuan-TFSI has a large electrochemical window and is able to reversibly plate and strip lithium. Thus, it is promising as a new electrolyte in lithium ion batteries. Its performance in a half cell equals that of commercial electrolytes at low C-rates or at elevated temperatures. As PipGuan-TFSI outperforms other common guanidinium and piperidinium based ionic liquids with regard to achieved capacities of $LiFePO_4$ half cells, the synthesis goal has been exceeded. The approach of target oriented “genetic crossing” of structural elements in IL molecules is a promising complement to computational screening and incremental modification of existing ILs. We expect this approach to trigger further improvements in the development of advanced electrolytes in the near future.

Acknowledgements

The authors would like to thank Mr. Jan Geder for helping with the TGA-MS measurements, Ms. Shubha Nageswaran for fruitful and interesting discussions regarding the work described in this article, and Mr. Xiaohan Wu for his help in conducting the experiments. The authors would also like to thank SOLVAY SA for providing the LiTFSI-salt. Maria Arkhipova thanks the State of Baden-Wuerttemberg for a graduate fellowship. This work was financially supported by the Singapore National Research Foundation under its Campus for Research Excellence and Technological Enterprise (CREATE) programme.

Notes and references

[a] *TUM CREATE, Singapore 138602, Singapore. Tel: +65 9455 3973; E-mail: harry.hoster@tum-create.edu.sg*
[b] *Technische Universität München, 85748 Garching,Germany.*
[c] *School of Materials Science and Engineering, Nanyang Technological University, Singapore 639798, Singapore.*
[d] *Energy Research Institute @ NTU, 1 CleanTech Loop, #06-04 CleanTech One, Singapore 637141.*
[e] *Institute of Organic Chemistry I, University of Ulm, Albert-Einstein-Allee 11, 89081 Ulm, Germany.*

# Authors contributed equally to this manuscript

1. A.-O. Diallo, A. B. Morgan, C. Len, and G. Marlair, *Energy Environ. Sci.*, 2013, **6**, 699.

2. H. Ohno, *Electrochemical Aspects of Ionic Liquids*, John Wiley & Sons, Inc., Hoboken, NJ, USA, 2005.

3. P. Wasserscheid and T. Welton, *Ionic Liquids in Synthesis*, Wiley-VCH Verlag GmbH & Co. KGaA, Weinheim, Germany, 2007.

4. N. MacDowell, N. Florin, A. Buchard, J. Hallett, A. Galindo, G. Jackson, C. S. Adjiman, C. K. Williams, N. Shah, and P. Fennell, *Energy Environ. Sci.*, 2010, **3**, 1645.

5. X. Zhang, X. Zhang, H. Dong, Z. Zhao, S. Zhang, and Y. Huang, *Energy Environ. Sci.*, 2012, **5**, 6668.

6. J. F. Wishart, *Energy Environ. Sci.*, 2009, **2**, 956.

7. M. Galiński, A. Lewandowski, and I. Stępniak, *Electrochim. Acta*, 2006, **51**, 5567–5580.

8. M. Armand, F. Endres, D. R. MacFarlane, H. Ohno, and B. Scrosati, *Nat. Mater.*, 2009, **8**, 621–629.

9. A. Lewandowski and A. Świderska-Mocek, *J. Power Sources*, 2009, **194**, 601–609.

10. H. Sakaebe, H. Matsumoto, and K. Tatsumi, *Electrochim. Acta*, 2007, **53**, 1048–1054.

11. F. Endres, *Phys. Chem. Chem. Phys.*, 2012, **14**, 5008–9.

12. S. Passerini and W. A. Henderson, in *Encyclopedia of Electrochemical Power Sources*, ed. J. Garche, Elsevier B.V., 2009, vol. 5, pp. 85–91.

13. C. H. Hamann, A. Hamnett, and W. Vielstich, *Electrochemistry*, Wiley VCH, Weinheim, 2007, vol. 2.

14. E. I. Izgorodina, *Phys. Chem. Chem. Phys.*, 2011, **13**, 4189–207.

15. J. Scheers, P. Johansson, and P. Jacobsson, *J. Electrochem. Soc.*, 2008, **155**, A628.

16. P. Johansson, L. E. Fast, A. Matic, G. B. Appetecchi, and S. Passerini, *J. Power Sources*, 2010, **195**, 2074–2076.

17. A. Fernicola, F. Croce, B. Scrosati, T. Watanabe, and H. Ohno, *J. Power Sources*, 2007, **174**, 342–348.

18. S. Seki, Y. Ohno, Y. Kobayashi, H. Miyashiro, A. Usami, Y. Mita, H. Tokuda, M. Watanabe, K. Hayamizu, S. Tsuzuki, M. Hattori, and N. Terada, *J. Electrochem. Soc.*, 2007, **154**, A173–A177.

19. J. Jin, H. H. Li, J. P. Wei, X. K. Bian, Z. Zhou, and J. Yan, *Electrochem. commun.*, 2009, **11**, 1500–1503.

20. V. Borgel, E. Markevich, D. Aurbach, G. Semrau, and M. Schmidt, *J. Power Sources*, 2009, **189**, 331–336.

21. M. Montanino, F. Alessandrini, S. Passerini, and G. B. Appetecchi, *Electrochim. Acta*, 2013, **96**, 124–133.

22. M. Egashira, S. Okada, J. Yamaki, D. A. Dri, F. Bonadies, and B. Scrosati, *J. Power Sources*, 2004, **138**, 240–244.

23. J. Sun, M. Forsyth, and D. R. MacFarlane, *J. Phys. Chem. B*, 1998, **102**, 8858–8864.

24. S. Fang, Z. Zhang, Y. Jin, L. Yang, S. Hirano, K. Tachibana, and S. Katayama, *J. Power Sources*, 2011, **196**, 5637–5644.

25. A. P. Lewandowski, A. F. Hollenkamp, S. W. Donne, and A. S. Best, *J. Power Sources*, 2010, **195**, 2029–2035.

26. T. Waldmann, H.-H. Huang, H. E. Hoster, O. Höfft, F. Endres, and R. J. Behm, *Chemphyschem*, 2011, **12**, 2565–7.

27. S. Fang, L. Yang, J. Wang, H. Zhang, K. Tachibana, and K. Kamijima, *J. Power Sources*, 2009, **191**, 619–622.

28. W. Kantlehner, E. Haug, W. W. Mergen, P. Speh, T. Maier, J. J. Kapassakalidis, H.-J. Braeuner, and H. Hagen, *Liebigs Ann. der Chemie*, 1984, 108–126.

29. Y. Jin, S. Fang, L. Yang, S. Hirano, and K. Tachibana, *J. Power Sources*, 2011, **196**, 10658–10666.

30. S. Fang, L. Yang, C. Wei, C. Jiang, K. Tachibana, and K. Kamijima, *Electrochim. Acta*, 2009, **54**, 1752–1756.

31. M. Gnahm, C. Berger, M. Arkhipova, H. Kunkel, T. Pajkossy, G. Maas, and D. M. Kolb, *Phys. Chem. Chem. Phys. PCCP*, 2012, **14**, 10647–10652.

32. X. Zhang, S. Fang, Z. Zhang, and L. Yang, *Chinese Sci. Bull.*, 2011, **56**, 2906–2910.

33. H. Kunkel and G. Maas, *European J. Org. Chem.*, 2007, **2007**, 3746–3757.

34. M. Montanino, M. Carewska, F. Alessandrini, S. Passerini, and G. B. Appetecchi, *Electrochim. Acta*, 2011, **57**, 153–159.

35. J. Reiter, M. Nádherná, and R. Dominko, *J. Power Sources*, 2012, **205**, 402–407.

36. K. Liu, Y.-X. Zhou, H.-B. Han, S.-S. Zhou, W.-F. Feng, J. Nie, H. Li, X.-J. Huang, M. Armand, and Z.-B. Zhou, *Electrochim. Acta*, 2010, **55**, 7145–7151.

37. O. O. Okoturo and T. J. VanderNoot, *J. Electroanal. Chem.*, 2004, **568**, 167–181.

38. M. L. F. Nascimento and C. Aparicio, *Phys. B Condens. Matter*, 2007, **398**, 71–77.

39. A. a. J. Torriero, J. Sunarso, and P. C. Howlett, *Electrochim. Acta*, 2012, **82**, 60–68.

40. P. Reale, A. Fernicola, and B. Scrosati, *J. Power Sources*, 2009, **194**, 182–189.

41. J. Hassoun, A. Fernicola, M. A. Navarra, S. Panero, and B. Scrosati, *J. Power Sources*, 2010, **195**, 574–579.

42. P. C. Howlett, N. Brack, A. F. Hollenkamp, M. Forsyth, and D. R. MacFarlane, *J. Electrochem. Soc.*, 2006, **153**, A595.

43. P. C. Howlett, D. R. MacFarlane, and A. F. Hollenkamp, *Electrochem. Solid-State Lett.*, 2004, **7**, A97.

44. L. Suo, Y.-S. Hu, H. Li, M. Armand, and L. Chen, *Nat. Commun.*, 2013, **4**, 1481.

45. P. De Vreese, K. Haerens, E. Matthijs, and K. Binnemans, *Electrochim. Acta*, 2012, **76**, 242–248.

46. A. Lewandowski, L. Waligora, and M. Galinski, *Electroanalysis*, 2009, **21**, 2221–2227.

47. D. Weingarth, a. Foelske-Schmitz, a. Wokaun, and R. Kötz, *Electrochem. commun.*, 2012, **18**, 116–118.

48. J. Thevenin, *J. Power Sources*, 1985, **14**, 45–52.

49. S. Seki, Y. Ohno, H. Miyashiro, Y. Kobayashi, A. Usami, Y. Mita, N. Terada, K. Hayamizu, S. Tsuzuki, and M. Watanabe, *J. Electrochem. Soc.*, 2008, **155**, A421.

50. H. Matsumoto, H. Sakaebe, K. Tatsumi, M. Kikuta, E. Ishiko, and M. Kono, *J. Power Sources*, 2006, **160**, 1308–1313.